

# Constraining inputs to realistic kilonova simulations through comparison to observed $r$ -process abundances

M. Ristic,<sup>1</sup> E. M. Holmbeck,<sup>2,3,4</sup> R. Wollaeger,<sup>5,6</sup> O. Korobkin,<sup>5,6</sup> E. Champion,<sup>7</sup> R. O’Shaughnessy,<sup>1</sup> C. L. Fryer,<sup>5,6,8,9</sup> C. J. Fontes,<sup>5,10</sup> M. R. Mumpower,<sup>4,5,11</sup> and T. M. Sprouse<sup>4,5,11</sup>

<sup>1</sup>*Center for Computational Relativity and Gravitation, Rochester Institute of Technology, Rochester, New York 14623, USA*

<sup>2</sup>*Observatories of the Carnegie Institution for Science, Pasadena, CA 91101, USA*

<sup>3</sup>*Hubble Fellow*

<sup>4</sup>*Joint Institute for Nuclear Astrophysics—Center for the Evolution of the Elements, USA*

<sup>5</sup>*Center for Theoretical Astrophysics, Los Alamos National Laboratory, Los Alamos, NM, 87545, USA*

<sup>6</sup>*Computer, Computational, and Statistical Sciences Division, Los Alamos National Laboratory, Los Alamos, NM, 87545, USA*

<sup>7</sup>*Department of Physics and Astronomy, University of Rochester, Rochester, NY 14627, USA*

<sup>8</sup>*The University of Arizona, Tucson, AZ 85721, USA*

<sup>9</sup>*Department of Physics and Astronomy, The University of New Mexico, Albuquerque, NM 87131, USA*

<sup>10</sup>*Computational Physics Division, Los Alamos National Laboratory, Los Alamos, NM, 87545, USA*

<sup>11</sup>*Theoretical Division, Los Alamos National Laboratory, Los Alamos, NM 87545, USA*

(Dated: October 12, 2022)

Kilonovae, one source of electromagnetic emission associated with neutron star mergers, are powered by the decay of radioactive isotopes in the neutron-rich merger ejecta. Models for kilonova emission consistent with the electromagnetic counterpart to GW170817 predict characteristic abundance patterns, determined by the relative balance of different types of material in the outflow. Assuming the observed source is prototypical, this inferred abundance pattern in turn must match  $r$ -process abundances deduced by other means, such as what is observed in the solar system. We report on analysis comparing the input mass-weighted elemental compositions adopted in our radiative transfer simulations to the mass fractions of elements in the Sun. We characterise the extent to which our parameter inference results depend on our assumed composition for the dynamical and wind ejecta and examine how the new results compare to previous work. We find that a dynamical ejecta composition calculated using the FRDM2012 nuclear mass and FRLDM fission models with extremely neutron-rich ejecta ( $Y_e = 0.035$ ) along with our “wind2” moderately neutron-rich ( $Y_e = 0.27$ ) wind ejecta composition yields a high mass ratio of  $M_w/M_d = 2.81$  which best matches the observed AT2017gfo kilonova light curves while also producing the best-matching abundance of neutron-capture elements in the solar system.

## I. INTRODUCTION

For nearly half a century, neutron star binaries have been known to exist in nature, stemming from the first detection of a binary pulsar system [1]. Shortly thereafter, the general relativistic prediction of gravitational radiation from a compact object binary was measured in the same system, implying the possibility of neutron star binary coalescence [2]. Recently, neutron star mergers were confirmed as astrophysical sources of both gravitational wave and electromagnetic emission with the detection of the binary neutron star merger GW170817 and its transient electromagnetic counterpart AT2017gfo [3–7].

Around the same time as the first pulsar binary detection, compact object mergers involving neutron stars, either binary neutron star (BNS) or black-hole-neutron-star (BHNS), were predicted to be candidates for rapid neutron capture ( $r$ -process) nucleosynthesis [8–11]. The nuclei synthesized in the immediate aftermath of the post-merger ejecta were thought to be heavy ( $A > 140$ ), with a sizeable fraction of radioactive isotopes which have short lifetimes due to their instability [12]. As these nuclei decayed, they would release energy into the surrounding matter which would be emitted as ultraviolet, optical, and infrared thermal radiation once the ejecta

became optically thin [13–15]. This thermal emission is now commonly referred to as a kilonova [16] and serves as the bridge between the  $r$ -process elements produced by neutron star mergers and their resultant electromagnetic emission [17–21]. Aside from the transient electromagnetic kilonova emission (including a gamma-ray burst [22, 23]),  $r$ -process material ejecta from neutron star binary mergers like GW170817 could produce another observable signature: relic  $r$ -process abundances such as in ancient, metal-poor stars and in our solar system.

Modeling kilonova light curves from merger events as viewed from the solar system by a distant observer requires the ejecta mass, velocity, composition, morphology, and viewing angle to be known, or otherwise supplied as model inputs. It has been conclusively demonstrated that the multiband light curves of AT2017gfo are poorly fit with single-component models, i.e., models consisting of a single type of ejecta described by fixed velocity, mass, and composition [24]. Instead, the AT2017gfo light curve is better fit by two (or even three) components describing multiple types of ejecta: generally, a high-opacity “dynamical” component, and a low-opacity “wind” component [7, 24–26].

In two-component models of kilonovae, the low-opacity wind component typically includes elements only up to

the “second  $r$ -process peak” at  $A \sim 130$ , while the higher-opacity dynamical component includes even heavier elements [27–29]. While these composition trends set a general opacity scale (see e.g., [30]), the full details of the composition effects on electromagnetic emission depend on the components’ nuclear physics considerations as well as their physical parameterizations described, in part, by the components’ masses  $M_d, M_w$  and velocities  $v_d, v_w$ , where “d” and “w” refer to the dynamical and wind components, respectively. Previous studies of kilonovae have highlighted the importance of nuclear physics inputs on  $r$ -process nucleosynthesis and the resultant effect on observed kilonova emission [31, 32]. In this work, we build on previous studies by considering the effect that nuclear physics uncertainties have on parameter inference from kilonova light curves.

This work presents two-component nucleosynthetic yield constraints assuming  $r$ -process contribution exclusively from neutron star mergers and electromagnetic constraints assuming all neutron star mergers are phenomenologically similar to GW170817. We investigate the effects of comparing elemental abundances from kilonova simulations to solar  $r$ -process abundances under the assumption that the second ( $A \sim 130$ ) and third ( $A \sim 195$ )  $r$ -process peaks follow universal behavior. We use this comparison to create a parameter estimation prior driven by explicit consideration of  $r$ -process elemental abundances in kilonova ejecta to gauge the effects on recovered ejecta properties; i.e., the masses and velocities of the ejecta components. As kilonova models improve in complexity and more observations become available for parameter estimation purposes, we can use more representative simulation abundances to hone this prior in future studies.

In this work, we will assess the extent to which our assumptions about the ejected material are simultaneously consistent with both types of aforementioned observations. Specifically, we will examine whether the abundances produced by our nucleosynthesis simulations realistically match the  $r$ -process abundances observed in the Sun while simultaneously reproducing the AT2017gfo light curve as well. In Section II A, we discuss the radiative transfer, atomic, and nuclear physics codes used to calculate the surrogate light curves, line-binned opacities, and ejecta compositions, respectively, considered in this work. In Section II B, we describe our method of comparing mass-weighted  $r$ -process abundances from our simulations with the solar abundance pattern. Section II C describes our parameter estimation framework and the effects of the  $r$ -process prior introduced in this work. In Section III we discuss whether the inclusion of the  $r$ -process prior makes a substantial difference in the parameter estimation process compared to prior work.

## II. METHODS

### A. Simulation Setup

The aforementioned abundances are not enough to create a direct link to kilonova electromagnetic emission on their own. However, they restrict which radioactive isotopes can plausibly exist and determine the radioactive heating rates powering the kilonova at different times. In this section, we describe the details of our ejecta compositions, the relevant thermalization efficiencies, and the composition-dependent ejecta opacity effects which all make up our kilonova emission model.

Throughout this work, we assume a two-component kilonova model composed of a lanthanide-rich “dynamical” ejecta component and a lanthanide-poor “wind” ejecta component. Each of our two ejecta components, dynamical and wind, is described by a fixed morphology and elemental composition. The morphologies are fixed to torus-shaped and peanut-shaped for the dynamical and wind ejecta, respectively (as defined in Ref. [33]). The wind component compositions, contributing to elements around and between the first ( $A \sim 80$ ) and second ( $A \sim 130$ )  $r$ -process peaks, are fixed in this study and are described by the H5 and H1 tracers in Ref. [34] for the “wind1” and “wind2” models, respectively. We consider two different wind models with lower (wind1) and higher (wind2) neutron-richness to gauge the effects of lighter and heavier element contributions in our comparison to solar  $r$ -process abundances. The dynamical ejecta compositions, composed of the elements from the second to the third  $r$ -process peak and beyond, are varied as described in Table I; the dynamical ejecta composition used in our previous study, marked with the (\*) label, is described by the model B tracer in [35].

We use the models from our previous study (see Ref. [36]) using SuperNu, a Monte Carlo code for simulation of time-dependent radiation transport with matter in local thermodynamic equilibrium [37]. Our light-curve simulations use radioactive power sources calculated from decaying the  $r$ -process composition from the WinNet code [38]. The contributions from these power sources are weighted by thermalization efficiencies first presented in [39] (see Ref. [40] for a detailed description of the adopted nuclear heating). We utilize detailed opacity calculations from the tabulated binned opacities generated using the Los Alamos suite of atomic physics codes [41, 42]. Our tabulated binned opacities are not calculated for all elements; therefore, we produce opacities for representative proxy elements by combining pure-element opacities of nuclei with similar atomic properties [42]. Our final SuperNu outputs are simulated kilonova spectra evaluated at 1024 equally log-spaced wavelength bins from  $0.1 \mu\text{m}$  to  $12.8 \mu\text{m}$  across 54 viewing angles spaced equally in  $\cos\theta$  for  $-1 \leq \cos\theta \leq 1$ . These spectra are then post-processed into light curves assuming a source distance of 10 parsecs.

Our SuperNu simulations require discrete mass and av-

erage outflow velocity parameter inputs for the ejecta components. To sample our parameter space continuously during parameter inference, we require a continuous mapping of ejecta parameter inputs to kilonova light curve outputs in the form of a Gaussian process surrogate model. We built our surrogate model training library of  $\sim 450$  kilonova light curve simulations using iterative simulation placement guided by Gaussian process variance minimization. In other words, we placed new simulations in regions of parameter space where our interpolation root-mean-square (RMS) uncertainty was largest. For simulation placement purposes, we only examined the uncertainty on the entire bolometric light curve rather than uncertainty at individual simulation times (see Ref. [36] for a full discussion on the creation of the simulation library).

Using Gaussian process regression interpolation in conjunction with our simulation library [36], we created a continuous mapping of our four ejecta parameter simulation inputs ( $M_d$ ,  $v_d$ ,  $M_w$ ,  $v_w$ ) to a scalar output  $M_{AB,\lambda}$  at some time  $t$ , angle  $\theta$ , and wavelength  $\lambda$ . Because of the substantial dynamic range of our many outputs, we interpolate in AB magnitudes using the LSST *grizy* and 2MASS *JHK* bands as our reference wavelengths. Our Gaussian process uses a squared-exponential kernel and a white noise (diagonal) kernel. Unless otherwise noted, we quantify the performance of our interpolation with the RMS difference between our prediction and the true value.

Combining our surrogate light curves and parameter inference code, we generated posteriors for the ejecta parameters of GW170817 given our model assumptions [36]. We perform four-dimensional Monte Carlo integration of the electromagnetic likelihood over our model’s four parameters using the EM\_PE package<sup>1</sup> to provide the likelihood and the RIFT adaptive Gaussian mixture model integrator to perform the integration [43]. The parameter estimation in this work, discussed in Section II C, follows the same methodology as in Ref. [36], with the additional composition-based prior constraint described in Section II B.

In creating our surrogate model light-curve training library, we considered only one dynamical ejecta composition and one wind ejecta composition, indicated by the (\*) label in Table I. The wind compositions in this work are unchanged from previous studies [33, 36, 40] while new considerations for dynamical ejecta compositions with different nuclear physics inputs were included in addition to the original dynamical composition used in prior studies. As a result of its ejection process, dynamical ejecta typically has a much lower electron fraction  $Y_e \equiv (n_p)/(n_p + n_n)$ , where  $n_p$  is the number of protons and  $n_n$  is the number of neutrons in the ejecta. A low electron fraction results in a higher availability of neutrons for capture during  $r$ -process nucleosynthesis and

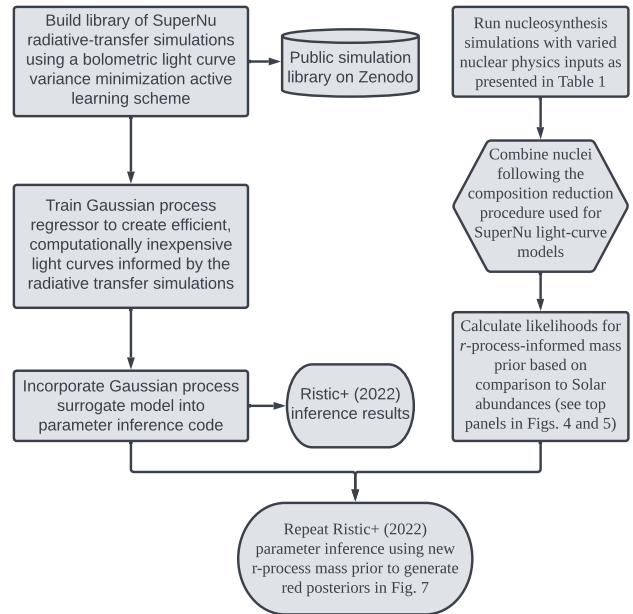


FIG. 1. Unified Modeling Language (UML) diagram describing the large-scale steps taken in creating the  $r$ -process mass prior and using it during parameter inference to generate the red posteriors in Figure 7. Per standard UML definition, rectangles represent processes, cylinders represent databases, hexagons represent data preparation steps and ovals represent terminators, or final products.

thus generally the creation of heavier elements such as lanthanides and actinides [44, 45]. Due to the dynamical ejecta’s dominance on the elemental abundance pattern compared to the relatively minimal contribution of the wind ejecta, we only present newly calculated compositions for dynamical ejecta in this work.

The compositions presented in this work were generated using two nuclear network codes: WinNet and PRISM. The dynamical and wind ejecta compositions considered here and in previous work (i.e. [36, 40]) were generated using WinNet. Specifically, these are the wind1 and wind2 compositions and the dynamical ejecta model using the Panov+ (2010) fission model in Table I.

The varied dynamical ejecta compositions new to this work were generated using PRISM. PRISM is a single-zone nuclear reaction network code that evolves an initial seed abundance of nuclei along a time-temperature-density thermodynamic trajectory, while allowing full flexibility with the input nuclear data [50]. In this work, we use state-of-the-art nuclear reaction and decay rates that are calculated to be self-consistent with the nuclear mass model. Following from the thermodynamic trajectories of dynamical ejecta from neutron star merger simulations presented in Ref. [20], all of our PRISM runs begin in nuclear statistical equilibrium at a temperature of 10 GK in the thermodynamic trajectory. All dynamical ejecta models presented in Table I with a fission model different from Panov+ (2010) were generated using PRISM.

<sup>1</sup> [github.com/markoris/EM\\_PE](https://github.com/markoris/EM_PE)

Mass Model	Fission Model	$Y_e$ $\left(\frac{n_p}{n_p+n_n}\right)$	Wind Comp.	Mass Ratio $(M_w/M_d)$	Min. Residual $(r_{\min})$
FRDM2012	FRLDM	0.035	wind2	2.81	355
FRDM2012	50/50	0.180	wind2	1.60	684
FRDM2012 (*)	Panov+ (2010)	0.035	wind2	1.76	784
HFB24	FRLDM	0.180	wind2	1.60	832
HFB24	FRLDM	0.035	wind2	4.09	865
FRDM2012	FRLDM	0.035	wind1	0.32	927
HFB24	FRLDM	0.035	wind1	0.10	1436
FRDM2012	50/50	0.180	wind1	1.21	1474
FRDM2012	Panov+ (2010)	0.035	wind1	13.90	2079
HFB24	FRLDM	0.180	wind1	9.54	2144

TABLE I. Wind-to-dynamical mass ratios sorted by increasing minimum residuals for each dynamical composition considered. Mass ratios were determined by calculating the mean mass ratio of the bottom 2nd percentile of all residuals so as to eliminate outliers. The residuals were calculated as in Equation 1 and the minimum residual was identified as the smallest residual across all the mass pairs considered for a given composition. The two wind1 and wind2 trajectories are described in detail in Ref. [40]. The two nuclear mass models considered are FRDM2012 and HFB24 [46, 47]. The two nuclear fission models considered in our study are FRLDM [48] and “50/50,” a simple symmetric assumption that fission yields split into two identical nuclei. The fission rates for the simulations performed in previous work, labeled Panov+ (2010), are taken from Ref. [49]. The (\*) indicates the compositions used in creating the surrogate light curves used during parameter estimation (see Section III).

The mass fractions of all the compositions considered in this work are shown in Figure 2. Figure 2 highlights the main difference between our wind ejecta compositions: the wind1 composition has very low mass fractions at the second  $r$ -process peak ( $A \sim 130$ ) while a significant portion of the wind2 composition is made up of elements around this peak.

### B. Ejecta Prior Implied by $r$ -process Observations

In our SuperNu simulations, we adopt a two-component compositional model and vary the mass ratio of the two components: the dynamical ( $M_d$ ) and wind ( $M_w$ ) ejecta masses. Each component has a fixed isotopic abundance, computed via nucleosynthesis network [38]. Due to the fixed nature of the compositions, we weight each component’s composition, represented by mass fractions  $X_d$  and  $X_w$ , by the mass of the respective ejecta component, dynamical  $M_d$  and wind  $M_w$ , to introduce composition variation as a function of component mass in the combined simulation mass fraction  $X_{\text{sim}} = (M_d X_d + M_w X_w)/(M_d + M_w)$ . For every isotope, the combined mass fraction  $X_{\text{sim}}$  is simply the mass-weighted sum of its mass fractions in the constitutive components. We varied our dynamical and wind component masses over a grid between  $-3 \leq \log(M_{d,w}/M_\odot) \leq -1$ , encompassing the most realistic ejecta masses predicted by numerical relativity simulations of neutron star mergers [29, 34, 51–54].

We seek to compare the combined mass fractions  $X_{\text{sim}}$  to the seemingly universal pattern of elements between the 2nd and 3rd  $r$ -process peaks (the “main”  $r$ -process,

[21]) observed among some old stars. This “ $r$ -process universality” has been noted for iron-poor (or “metal-poor”) stars that show enhancements in the main  $r$ -process elements relative to their iron content in excess of ten times the equivalent Solar ratio. However, observationally derived abundances in metal-poor stars are necessarily elemental since the abundances are derived from atomic transitions in stellar spectra that are overall insensitive to atomic mass number. Except for a handful of elements, the detailed *isotopic* distributions of  $r$ -process elements in metal-poor stars is observationally unknown. As a proxy for a representative example of the universal  $r$ -process, we use the well-studied solar isotopic abundance pattern  $X_\odot$ , relying on previously-published projections of the high- $A$  elements into different neutron-capture process contributions. Specifically, the  $r$ -process fractions presented in Ref. [55] are used in conjunction with the total abundances from Ref. [56] to isolate the contribution to the solar abundances by the  $r$ -process.

Figure 3 shows the  $[X/\text{Fe}]$  abundances of six metal-poor stars. The “[X/Fe]” notation means that each elemental ratio  $\log \epsilon(X/\text{Fe})$  is compared to the same elemental ratio in the solar abundance pattern.<sup>2</sup> Stars with  $[X/\text{Fe}] > 0$  are considered “enhanced” in that element relative to the solar system abundance. For many metal-poor stars, elements with  $Z \geq 37$  have an enhanced abundance compared to iron. For this work, guided by the enhancement seen in elements  $Z \geq 37$  in Figure 3

<sup>2</sup> Definition:  $[X/\text{Fe}] := \log \epsilon(X/\text{Fe}) - \log \epsilon(X/\text{Fe})_\odot$ , where  $\log \epsilon(X) := \log_{10}(Y_X/Y_H) = \log_{10}(Y_X) + 12$ , where  $Y_X$  is the *abundance* (mole fraction) of the element X.

and with the assumption that iron was created during supernova nucleosynthesis, we assume that elements with  $Z \geq 37$  originate *exclusively* from neutron star mergers. The trends of elements with  $Z < 37$  are less clear; they are not uniformly enhanced in stars that are enhanced with the  $Z \geq 37$  elements, likely pointing to multiple (non-merger) origins for these elements.

To account for isotopes of actinides with short decay timescales, we rescale the solar mass fractions of actinides  $X_{\odot,Ac}$  to what they would have been at 1 day to better match the kilonova-timescale mass fractions used in our simulations. The rescaling is achieved by setting the 1-day solar actinide mass fractions to values that would decay to present day values after 4.5 Gyr. The rescaled solar mass fractions are also mapped into a subset of representative elements used for SuperNu light-curve modeling as described in Section II A. Hereafter, any mention of the solar mass-fraction pattern  $X_{\odot}$  refers to the 1-day rescaled and mapped mass fractions using data from Refs. [55] and [56].

To get  $X_{\odot}$  and  $X_{sim}$  on the same relative scale, we introduce an offset  $C_{scale,Z}$  that shifts  $X_{\odot}$  down to comparable values for  $X_{sim}$  by matching the two mass-fraction values at some element  $Z$ . To minimize how the choice of  $C_{scale,Z}$  affects our results, we integrate over the range of possible values of  $C_{scale,Z}$  introduced by scaling  $X_{\odot}$  and  $X_{sim}$  to matching values at different elements  $Z$ . This integration marginalizes over our uncertainty in  $C_{scale,Z}$ , adopting a Gaussian prior on  $\log(C_{scale,Z})$  with mean  $\mu = 1.61$  and variance  $\sigma^2 = 0.766$ . After integrating over  $C_{scale,Z}$ , we are left with a single required choice of a new  $C$  value that sets the constrained scale at some element  $Z_{choice}$  such that  $\log X_{sim,Z_{choice}} = \log X_{\odot,Z_{choice}} - \log C$ . We chose  $Z_{choice} = 46$  as it is one of the elements present in all the dynamical, wind, and solar mass fractions. Shifting  $X_{\odot}$  to be on the same relative scale as  $X_{sim}$  and choosing a specific value of  $C$  at some  $Z_{choice}$  are both done solely for the purpose of calculating well-behaved likelihoods. While the scaling by  $C$  removes the constraint that  $\sum_Z X_{\odot,Z} = 1$ , this has no detrimental effects on our analysis as we are interested exclusively in our compositions' relative abundances.

As part of our assumption that elements  $Z \geq 37$  were synthesized exclusively in neutron star mergers (see Figure 3), we only consider elements from  $Z = 37$  up to and including  $Z = 102$  when computing the residual  $r(M_d, M_w)$  for all available elements in the solar abundance pattern  $Z \in Z_{\odot}$  given a simulation with component masses  $M_d, M_w$ :

$$r(M_d, M_w) = \sum_{Z=37}^{102} \frac{(\log X_{\odot,Z} - \log C - \log X_{sim,Z})^2}{2\sigma^2} - \frac{N}{2\sigma^2} \frac{(\log \bar{X}_{sim} - \log \bar{X}_{\odot})^2}{1 + \sigma^2 / (N\sigma_C^2)} \quad (1)$$

where  $r(M_d, M_w)$  is the residual for the given dynamical

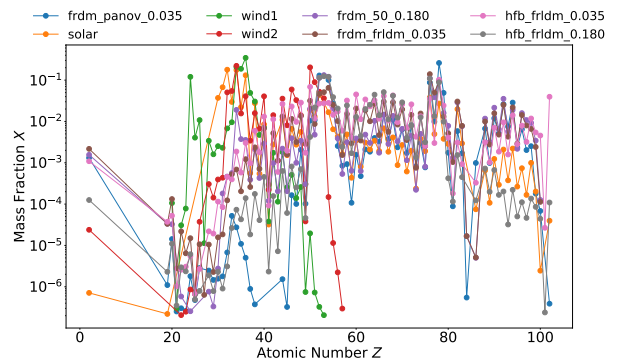


FIG. 2. Unscaled mass-fractions  $X$  as a function of atomic number  $Z$  for all compositions considered in this work. The labels pertaining to the dynamical ejecta compositions considered in this work indicate the nuclear mass model, fission model, and electron fraction  $Y_e$  used to generate the respective composition. The remaining labels indicate the solar and wind compositions. The wind1 and wind2 compositions do not extend to heavier atomic numbers  $Z$  due to their higher electron fractions  $Y_e = 0.37$  and  $Y_e = 0.27$ , respectively.

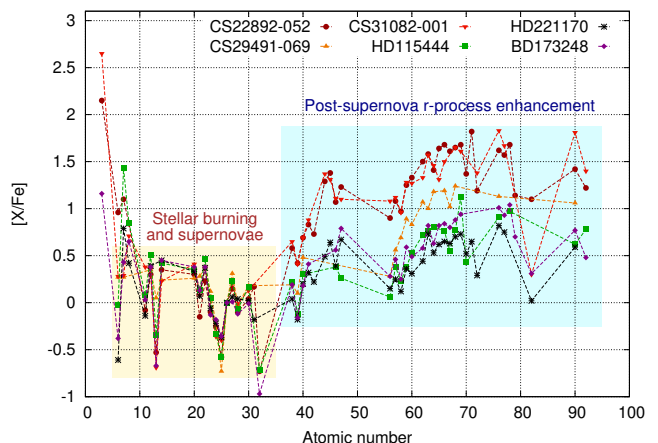


FIG. 3. Elemental mass fraction ratios relative to iron of a sample of  $r$ -process enriched metal-poor stars.  $[X/Fe] > 0$  implies enhanced abundance of element  $X$  compared to the solar system with respect to iron. We assume all elements that are significantly enhanced compared to iron to have been introduced post-supernova, exclusively from neutron star mergers. The region of enhanced elements ( $Z \geq 37$ , highlighted in blue) is the focus of our comparison to solar composition. The iron-peak elements and supernova  $r$ -process are not strongly enhanced compared to solar (highlighted in yellow). Stellar elemental abundances obtained from JINAbase [57] with the respective stars reported in references [58–63].

and wind mass pair used to calculate  $X_{sim} = (M_d X_d + M_w X_w) / (M_d + M_w)$ ,  $Z$  is the element's atomic number,  $\log X_{\odot,Z}$  is the decimal logarithm of the solar mass fraction of element  $Z$ ,  $\log C$  is the decimal logarithm of the offset matching  $X_{\odot}$  to  $X_{sim}$  at  $Z = 46$ ,  $\log X_{sim,Z}$  is the decimal logarithm of the simulation mass fraction of element  $Z$  in both components (if present),  $\sigma$  is the un-

certainty on  $\log X_{\text{sim}}$ ,  $\sigma_C$  is the uncertainty introduced by integrating out  $C_{\text{scale},Z}$ ,  $\bar{X}_{\odot}$  is the average solar mass fraction across all elements,  $\bar{X}_{\text{sim}}$  is the average simulation mass fraction across all elements, and  $N$  is the total number of elements considered.

We compute the residual between each of our composition models  $X_{\text{sim}}$  from Table I and the solar mass-fraction pattern  $X_{\odot}$  using Equation 1. We consider component mass weights across a log-spaced grid with  $-3 \leq \log(M_{d,w}/M_{\odot}) \leq -1$ , with 50 masses for each component resulting in a total of 2500 residuals per composition model. The likelihood  $\mathcal{L} = \exp(-0.003(r - r_{\text{min}}))$  for the 2500 residuals is shown in the top panel of Figures 4 and 5, with  $r$  representing the residual calculated for each mass pair and  $r_{\text{min}}$  the lowest residual for all mass pairs considered for a given model. The factor of 0.003 in the likelihood  $\mathcal{L}$  was introduced as a scaling factor to keep the large residuals well-behaved when evaluating the likelihood. The choice of scaling factor will directly affect the width of the likelihood peak and will influence how constraining the mass prior is during parameter inference.

### C. Parameter Inference

As in many previous applications of Bayesian inference to infer parameters of kilonovae [26, 64–70], we seek to compare the observed magnitudes  $x_i$  at evaluation points  $i$  (denoting a combination of band and time) to a continuous model that makes predictions  $m(i|\theta)$  which depend on some model parameters  $\theta$ . Bayes theorem expresses the posterior probability  $p(\theta)$  in terms of a prior probability  $p_{\text{prior}}(\theta)$  for the model parameters  $\theta$  and a likelihood  $\mathcal{L}(\theta)$  of all observations, given the model parameters, as

$$p(\theta) = \frac{\mathcal{L}(\theta)p_{\text{prior}}(\theta)}{\int d\theta \mathcal{L}(\theta)p_{\text{prior}}(\theta)}. \quad (2)$$

Unless otherwise noted, for simplicity we assume that the source sky location, distance, and merger time are known. We adopt a uniform prior on the ejecta velocity  $v/c \in [0.05, 0.3]$  and the two-dimensional prior discussed in Section II B on the ejecta masses  $m/M_{\odot} \in [0.001, 0.1]$ .

We assume the observations have Gaussian-distributed magnitude errors with presumed known observational (statistical) uncertainties  $\sigma_i$ , convolved with some additional unknown systematic uncertainty  $\sigma$ , so that our log-likelihood is

$$\ln \mathcal{L}(\theta) = -0.5 \sum_{i=1}^n \left[ \frac{(x_i - m(i|\theta))^2}{\sigma_i^2 + \sigma^2} + \ln(2\pi(\sigma_i^2 + \sigma^2)) \right] \quad (3)$$

where the sum is taken over every data point in every band used in the analysis. For inference using our Gaussian process surrogate models, we set  $\sigma$  to the estimated Gaussian process model error. For a full discussion of our parameter inference considerations, see Ref. [36].

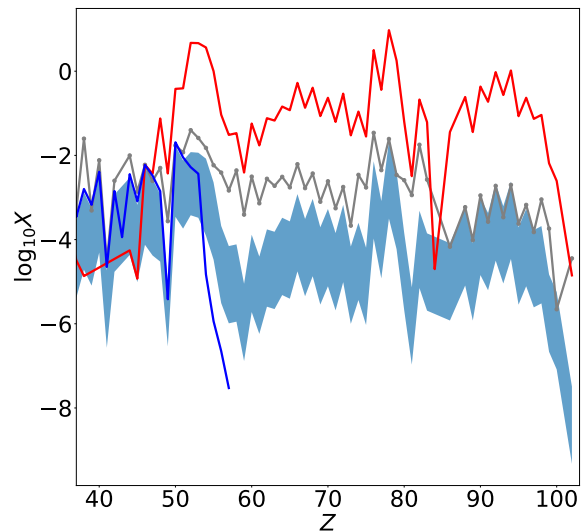
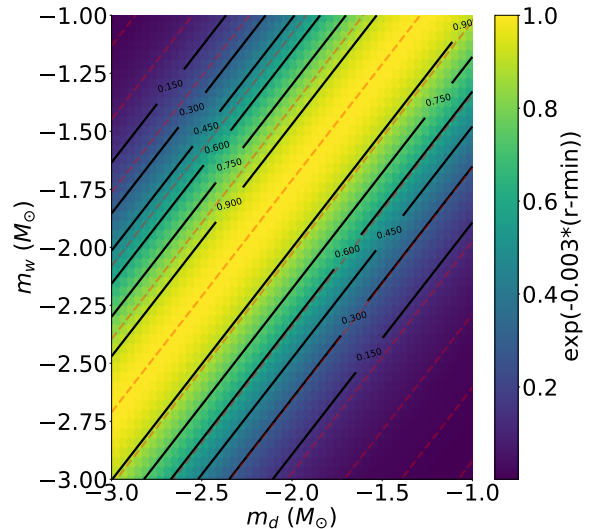


FIG. 4. *Top*: 2D distribution of likelihoods calculated as in Equation 1 by comparing  $\log X_{\odot}$  to  $\log X_{\text{sim}}$  using the dynamical and wind compositions matching those in [36], represented by the (\*) label in Table I. The likelihood grid is composed of 50 mass values equally log-spaced between  $-3 \leq \log M_{\odot} \leq -1$  for both dynamical and wind mass. The black lines indicate contours of equally-spaced likelihood values. The dashed red lines indicate a wind-to-mass ratio of 1 and serve purely as a visual aid. *Bottom*: Composition of individual components in terms of mass fractions  $X_Z$  compared to the mass fractions of the solar  $r$ -process residuals. The red and blue lines are the initial unweighted dynamical and wind ejecta mass fractions, respectively, scaled by  $C$  to match the solar mass fraction at  $Z = 46$ . The gray line is the solar mass fraction and the blue shaded region is the 90% confidence interval for all the mass-weighted mass fractions  $\log X_{\text{sim}}$ . The dynamical ejecta mass fraction only exceeds  $\log X = 1$  due to the scale matching at  $Z = 46$ .

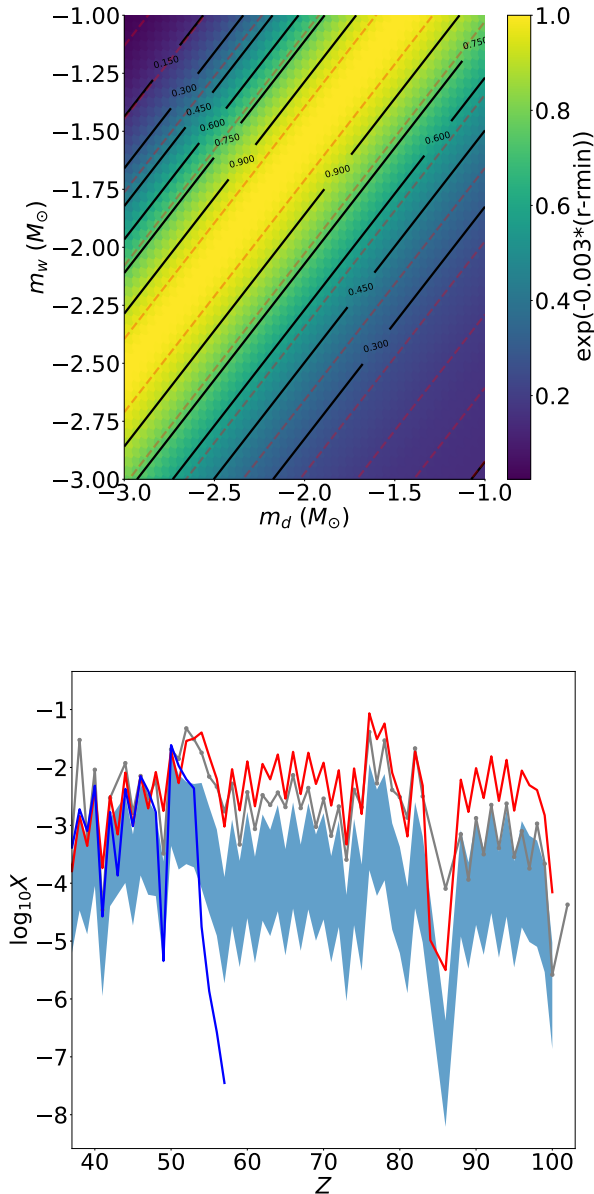


FIG. 5. *Top*: Same 2D distribution as described in Figure 4 except with the compositions which yielded the lowest residual in comparison to the solar abundance pattern (top row of Table I). *Bottom*: Composition of individual components in terms of mass fractions  $X_Z$  compared to the mass fractions of the solar  $r$ -process residuals. The line colors represent the same quantities as in Figure 4. The minimum residual was identified as the smallest residual across all the mass pairs considered for a given composition.

### III. RESULTS

For our two-component models, assuming a single source like GW170817 dominates the observed solar  $r$ -

process abundances, the inferred abundances from such mergers only depend on the mass ratio  $M_w/M_d$ . In other words, since in our study we emphasize only the relative and not absolute  $r$ -process abundances, motivated by considerable uncertainty in the binary neutron star merger rate, we therefore only use and constrain the abundance *ratios*. The relative abundances from a single channel only depend on the relative proportions of this channel; for our two-component model, this is simply dependent on  $M_w/M_d$ . Thus for each set of initial assumptions—the composition of the dynamical ejecta (represented by the electron fraction  $Y_e$ ), the presumed nuclear mass and fission model, and other details—our comparison with solar abundances necessarily constrains  $M_w/M_d$  narrowly around a preferred value unique to that model. We note that the abundances we are considering are effectively frozen out for the processes we’re interested in at times later than  $\mathcal{O}(1)$  second.

Table I provides a list of models and their preferred  $M_w/M_d$ , in the sense that they minimize the residual mismatch with the solar abundances as calculated in Equation 1. With a few exceptions, most models prefer  $M_w/M_d$  slightly above but close to unity. In other words, most of our abundance comparisons suggest somewhat more wind than dynamical ejecta would be required for GW170817-like mergers to reproduce the solar  $r$ -process abundances. These results are consistent with those found from other contemporary modeling [66, 69, 71, 72] as well as numerical relativity results [34, 54, 73–75].

The top panel of Figure 4 shows the likelihoods for the composition and morphology assumptions considered in previous work [36], denoted by the (\*) label in Table I. The yellow stripe indicating the highest likelihood region highlights the best-fitting ratio of wind-to-dynamical mass implied by the calculated residuals. This corresponds to the “Mass Ratio ( $M_w/M_d$ )” value recorded in Table I.

The top panel of Figure 5 shows the best-fitting wind-to-dynamical mass ratio for the lowest residual composition model presented in this work: dynamical ejecta with a composition characterized by the FRDM 2012 mass model, FRLDM fission model, electron fraction  $Y_e = 0.035$  and wind ejecta corresponding to the wind2 model. Resultantly, due to its constraining power on the preferred values of  $M_d$  and  $M_w$ , the top panel of Figure 5 functions as our newly introduced two-dimensional mass-weighted  $r$ -process composition prior on the ejecta masses.

The bottom panels of Figures 4 and 5 show the solar mass-fraction pattern  $X_\odot$  in gray, the dynamical and wind ejecta fixed composition mass-fraction patterns  $X_d$  and  $X_w$  in red and blue, respectively, and the 90% confidence interval for the mass-fraction pattern of the relevant composition model  $X_{\text{sim}}$  as the light-blue shaded region. The 90% confidence interval was calculated for the spread of possible mass-fraction patterns which arose when scaling the fixed component compositions  $X_d$  ( $X_w$ ) by the component mass  $M_d$  ( $M_w$ ).

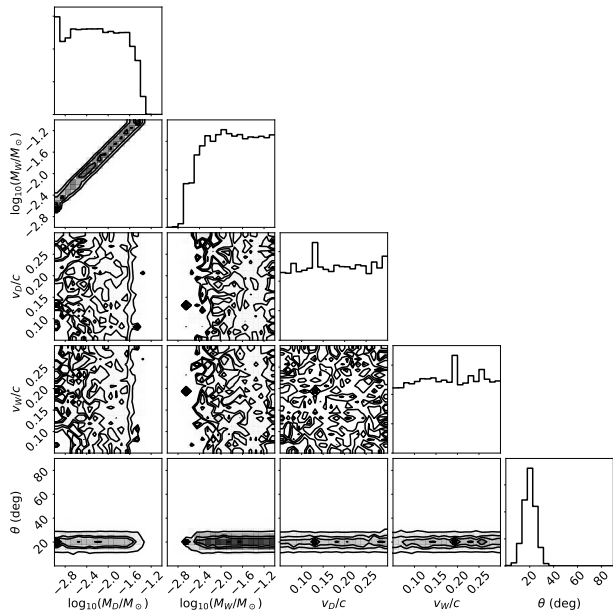


FIG. 6. Posterior distributions created using only the 2-D  $r$ -process prior presented in Figure 5 with no electromagnetic information provided during sampling besides constraints on the opening angle (see Ref. [76] and references therein). Note the recovery of the yellow band of lowest-residual mass pairs from Figure 5 in the  $M_w$  vs.  $M_d$  panel as well as the flat velocity posteriors stemming from the lack of velocity constraints introduced by our mass-focused prior. Residual small-scale substructure in the one- and two-dimensional marginal distributions reflects sample size artifacts. See Figure 7 for comparison.

For each set of initial assumptions, the inferred constraint on  $M_w/M_d$  therefore also strongly constrains the ingredients powering the associated kilonova. For example, Figure 6 shows the results of inferring the parameters of GW170817, using *only* our prior constraints on  $M_w/M_d$  from the top panel of Figure 5 (and weak constraints on the binary orientation relative to our line of sight). Figure 7 shows how these constraints propagate into joint electromagnetic inference. The solid black contours show inferences derived without using constraints on  $M_w/M_d$ ; the red contours show inferences supplemented with this insight, for a specific set of initial assumptions.

Each set of our input assumptions about ejecta composition and physics makes a prediction about  $r$ -process abundances. As shown by the last column in Table I, some of our input assumptions fit better than others. Given substantial systematic uncertainties associated in the many assumptions in our study, we approach these nominal residuals with considerable cautions. However, the minimum residuals presented in Table I suggest that the wind2 model is a notably better fit to the solar mass-fraction pattern, consistent with similar findings in previous studies [77]. The distinctly grouped separation of the

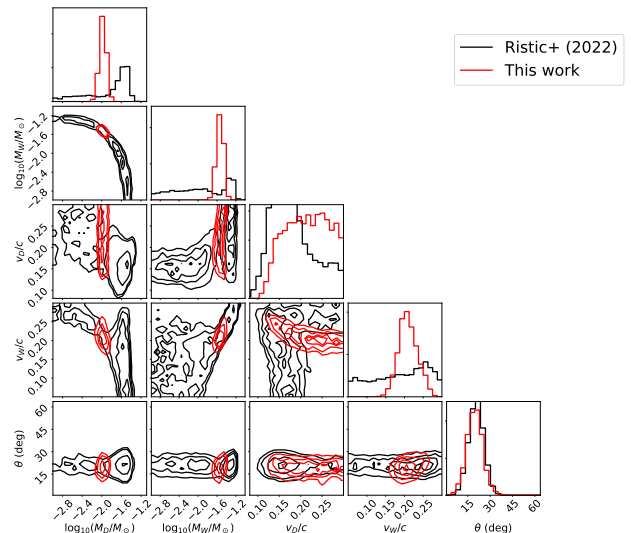


FIG. 7. Posterior distributions for samples generated when using the *grizyJHKS* bands considered in [36] (black) and samples generated using the same bands along with the  $r$ -process prior from Figure 5 (red). There is a clear shift in the recovered parameters with all but the dynamical velocity becoming more constrained.

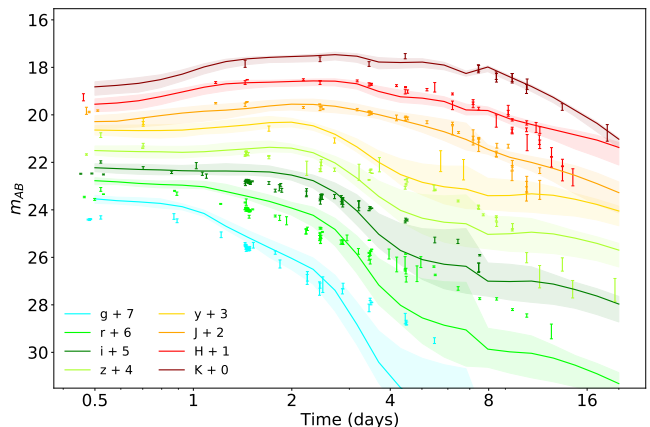


FIG. 8. Broadband light-curve predictions for the ejecta parameters recovered in Figure 7. The inclusion of the composition-based mass prior (top panel of Figure 5) relieves the tension in the bluer bands at late times compared to previous predictions [36].

two wind models' lowest residuals implies that the wind1 model is less indicative of  $r$ -process nucleosynthesis from neutron star mergers; however, our work neglects consideration of lighter  $r$ -process elements ( $Z \leq 37$ ) which disfavors compositions with higher  $Ye$  like wind1. More importantly, the separation between the models also implies that new models for the wind ejecta composition need to be considered in comparison to the wind2 model. The results of Table I indicate the need for further studies involving updated wind ejecta composition modeling



informed by GRMHD disk simulations [29].

However, the bottom panel of Figure 5 shows that, even for our lowest residual model, the solar mass-fraction  $X_{\odot}$  is still largely outside of our 90% confidence interval for  $X_{\text{sim}}$ . One possible explanation for this behavior is that we consider a simplified approach of attributing single  $Y_e$  values to each of our components instead of more realistic  $Y_e$  distributions as suggested by recent numerical relativity simulations [78, 79]. In the short term, the results of Table I will help parameter inference efforts constrain neutron star merger ejecta mass more tightly; however, future parameter estimation work will require a more detailed treatment of the ejecta  $Y_e$  to present a holistic picture of the post-merger scenario.

The results of Table I also depend strongly on the assumption that neutron star mergers are the *dominant*  $r$ -process mechanism for the creation of elements with  $Z \geq 37$  (see Figure 3 and Section II B), which may not be the case; see, e.g., Ref. [80] and references therein.

Our method as stated also assumes that a narrow distribution of mergers in total mass  $M_{\text{tot}} = M_1 + M_2$  dominates nucleosynthesis yields. While self-evidently consistent with the binary neutron star population inferred from the merging Galactic neutron star binaries, this assumption could even still hold for a wider binary neutron star population as suggested by gravitational wave observations, if ejecta are (as expected) suppressed for the most massive mergers with large  $M_{\text{tot}}$ .

Another caveat that presents limitations to our results is that we only incorporate very specific wind1 and wind2 compositions. There can be a broad variety of compositions permitted for electron fractions  $Y_e > 0.20$  due to varying hydrodynamic conditions. An extensive study of these compositions, along with the tests of how much they can be considered “representative” of their respective components, is beyond the scope of this work.

Our results can further be improved by incorporating the observed higher variability of the lighter  $r$ -process abundances between the first and the second peak, compared to the universal pattern between the second and third  $r$ -process peaks. The lighter  $r$ -process as observed in metal-poor stars, exhibits variation on the order of 1 dex, while the “strong”  $r$ -process pattern varies by only about 0.3 dex [21]. An investigation with more accurate numbers based on careful statistical analysis of observations will be the subject of future studies [81].

Finally, we note that we cannot ignore the bias introduced by the dynamical ejecta composition of the surrogate kilonova light curves presented in [36]. While the constraints imposed by the  $r$ -process abundance prior indeed shift the recovered parameters as in Figure 7, there still remains some contribution to the parameter estimation stemming from the surrogate models having been trained on a different dynamical ejecta composition. In other words, our surrogate light curves were trained using the ejecta compositions in Table I labeled with (\*). Although the primary contribution to the parameter inference in this work comes from the prior discussed in

Section II B, some bias from the surrogates’ original compositions is unavoidable.

#### IV. CONCLUSION

We have presented an approach for incorporating nuclear physics-based composition effects as a prior for our kilonova parameter inference framework. With the assumption that the general population of neutron star mergers will follow consistent  $r$ -process nucleosynthesis patterns, our approach allows for identification of best-fitting kilonova component compositions compared to the solar abundance. We considered a range of models with varying nuclear physics inputs, and, given the assumptions discussed above, the best-fitting model appears to be the one with FRDM2012 nuclear mass, FRLDM fission,  $Y_e = 0.035$  (extreme neutron richness in dynamical ejecta), wind2 moderately neutron-rich wind ejecta, producing inferred dynamical and wind ejecta masses of  $M_d \sim 0.01$  and  $M_w \sim 0.025$  and corresponding to a high mass ratio:  $M_w/M_d = 2.81$ . Our consideration of additional dynamical ejecta compositions, when compared to solar abundances, has indicated that the mass ratio between the two ejecta components is larger than what was implied by previous inference ( $M_w/M_d = 1.76$ ). However, our conclusions should be taken with care, since the number of input compositions considered were quite limited.

We have also shown that the inferred mass ratio stemming from a comparison of  $r$ -process elemental abundances is highly sensitive to the input nuclear physics. For our preferred wind2 model, variations in the dynamical ejecta composition can change the recovered wind-to-dynamical ejecta mass ratio by a factor of  $\sim 2.5$ . For the wind1 model, the inferred mass ratio can change by a factor of  $\sim 139$ , although this is largely due to the assumptions made in this work.

Even allowing for extremely conservative systematic uncertainties on our inputs (e.g., assuming  $M_w/M_d$ ’s optimal value is well-localized between 0.1 and 10), these prior abundance constraints should still provide useful insight into kilonova ejecta modeling. For instance, this framework of kilonova surrogates with abundance priors can be used as a constraint to identify merger simulations that produce consistent properties.

With the introduction of this composition-based prior, we are able to continue using our existing kilonova surrogate model and parameter inference frameworks while updating our inference priors to match contemporary results in the literature. The ability to update our mass prior using the underlying properties of kilonova models, without requiring expensive simulations (outside of nuclear network outputs), allows us to inexpensively and rapidly update our parameter inference results.

In this work, we have considered fiducial initial conditions for the outflow, including composition, without allowing for correlations induced by the fact that both

the composition and outflows are initialized by binary neutron star mergers. In future work, we will explore self-consistent initialization from merger properties, in particular exploring the effects of binary mass ratio and neutron star remnant lifetime, which should have significant impact on the ejecta amount and composition [82–84].

## V. ACKNOWLEDGMENTS

ROS, MR, and EMH acknowledge support from NSF AST 1909534. EMH acknowledges additional support for this work by NASA through the NASA Hubble Fellowship grant HST-HF2-51481.001, awarded by the Space Telescope Science Institute, which is operated by the

Association of Universities for Research in Astronomy, Inc., for NASA, under contract NAS5-26555. CJF, CLF, MRM, OK, RW, and TMS were supported by the US Department of Energy through the Los Alamos National Laboratory. Los Alamos National Laboratory is operated by Triad National Security, LLC, for the National Nuclear Security Administration of U.S. Department of Energy (Contract No. 89233218CNA000001). Research presented in this article was supported by the Laboratory Directed Research and Development program of Los Alamos National Laboratory under project number 20190021DR. This research used resources provided by the Los Alamos National Laboratory Institutional Computing Program, which is supported by the U.S. Department of Energy National Nuclear Security Administration under Contract No. 89233218CNA000001.

- 
- [1] R. A. Hulse and J. H. Taylor, “Discovery of a pulsar in a binary system.” *Astrophysical Journal Letters* **195**, L51–L53 (1975).
- [2] J. H. Taylor and J. M. Weisberg, “A new test of general relativity - Gravitational radiation and the binary pulsar PSR 1913+16,” *Astrophys. J.* **253**, 908–920 (1982).
- [3] The LIGO Scientific Collaboration, the Virgo Collaboration, B. P. Abbott, R. Abbott, T. D. Abbott, F. Acernese, K. Ackley, C. Adams, T. Adams, P. Addesso, *et al.*, “GW170817: Observation of gravitational waves from a binary neutron star inspiral,” *Phys. Rev. Lett.* **119**, 161101 (2017).
- [4] The LIGO Scientific Collaboration, the Virgo Collaboration, B. P. Abbott, R. Abbott, T. D. Abbott, F. Acernese, K. Ackley, C. Adams, T. Adams, P. Addesso, and *et al.*, “Estimating the Contribution of Dynamical Ejecta in the Kilonova Associated with GW170817,” *Astrophysical Journal Letters* **850**, L39 (2017), arXiv:1710.05836 [astro-ph.HE].
- [5] The LIGO Scientific Collaboration, the Virgo Collaboration, B. P. Abbott, R. Abbott, T. D. Abbott, F. Acernese, K. Ackley, C. Adams, T. Adams, P. Addesso, and *et al.*, “Multi-messenger Observations of a Binary Neutron Star Merger,” *Astrophysical Journal Letters* (2017), doi:10.3847/2041-8213/aa91c9.
- [6] The LIGO Scientific Collaboration, the Virgo Collaboration, B. P. Abbott, R. Abbott, T. D. Abbott, F. Acernese, K. Ackley, C. Adams, T. Adams, P. Addesso, and *et al.*, “On the Progenitor of Binary Neutron Star Merger GW170817,” *Astrophysical Journal Letters* **850**, L40 (2017), arXiv:1710.05838 [astro-ph.HE].
- [7] N. R. Tanvir, A. J. Levan, C. González-Fernández, O. Korobkin, I. Mandel, S. Rosswog, J. Hjorth, P. D’Avanzo, A. S. Fruchter, C. L. Fryer, *et al.*, “The emergence of a lanthanide-rich kilonova following the merger of two neutron stars,” *The Astrophysical Journal* **848**, L27 (2017).
- [8] J. M. Lattimer and D. N. Schramm, “Black-Hole-Neutron-Star Collisions,” *Astrophysical Journal Letters* **192**, L145 (1974).
- [9] J. M. Lattimer and D. N. Schramm, “The tidal disruption of neutron stars by black holes in close binaries.” *Astrophys. J.* **210**, 549–567 (1976).
- [10] E. Symbalisty and D. N. Schramm, “Neutron Star Collisions and the r-Process,” *Astrophysical Journal Letters* **22**, 143 (1982).
- [11] David Eichler, Mario Livio, Tsvi Piran, and David N. Schramm, “Nucleosynthesis, neutrino bursts and  $\gamma$ -rays from coalescing neutron stars,” *Nature (London)* **340**, 126–128 (1989).
- [12] Stephan Rosswog, “The multi-messenger picture of compact binary mergers,” *International Journal of Modern Physics D* **24**, 1530012-52 (2015), arXiv:1501.02081 [astro-ph.HE].
- [13] Li-Xin Li and Bohdan Paczyński, “Transient Events from Neutron Star Mergers,” *Astrophysical Journal Letters* **507**, L59–L62 (1998).
- [14] S. R. Kulkarni, “Modeling Supernova-like Explosions Associated with Gamma-ray Bursts with Short Durations,” arXiv e-prints , astro-ph/0510256 (2005), arXiv:astro-ph/0510256 [astro-ph].
- [15] B. D. Metzger, G. Martínez-Pinedo, S. Darbha, E. Quataert, A. Arcones, D. Kasen, R. Thomas, P. Nugent, I. V. Panov, and N. T. Zinner, “Electromagnetic counterparts of compact object mergers powered by the radioactive decay of r-process nuclei,” *Monthly Notices of the Royal Astronomical Society* , 840+ (2010).
- [16] Brian D. Metzger, “Kilonovae,” *Living Reviews in Relativity* **23** (2019), 10.1007/s41114-019-0024-0.
- [17] L. F. Roberts, D. Kasen, W. H. Lee, and E. Ramirez-Ruiz, “Electromagnetic Transients Powered by Nuclear Decay in the Tidal Tails of Coalescing Compact Binaries,” *Astrophysical Journal Letters* **736**, L21 (2011), arXiv:1104.5504 [astro-ph.HE].
- [18] Stephane Goriely, Andreas Bauswein, and Hans-Thomas Janka, “r-process Nucleosynthesis in Dynamically Ejected Matter of Neutron Star Mergers,” *Astrophysical Journal Letters* **738**, L32 (2011), arXiv:1107.0899 [astro-ph.SR].
- [19] B. D. Metzger and E. Berger, “What is the Most Promising Electromagnetic Counterpart of a Neutron Star Binary Merger?” *Astrophys. J.* **746**, 48 (2012).
- [20] O. Korobkin, S. Rosswog, A. Arcones, and C. Winteler, “On the astrophysical robustness of the neutron

- star merger r-process,” *Monthly Notices of the Royal Astronomical Society* **426**, 1940–1949 (2012).
- [21] John J. Cowan, Christopher Sneden, James E. Lawler, Ani Aprahamian, Michael Wiescher, Karlheinz Langanke, Gabriel Martínez-Pinedo, and Friedrich-Karl Thielemann, “Origin of the heaviest elements: The rapid neutron-capture process,” *Reviews of Modern Physics* **93**, 015002 (2021), arXiv:1901.01410 [astro-ph.HE].
- [22] B. P. Abbott, R. Abbott, T. D. Abbott, F. Acernese, K. Ackley, C. Adams, T. Adams, P. Addesso, R. X. Adhikari, V. B. Adya, and et al., “Gravitational Waves and Gamma-Rays from a Binary Neutron Star Merger: GW170817 and GRB 170817A,” *Astrophysical Journal Letters* **848**, L13 (2017), arXiv:1710.05834 [astro-ph.HE].
- [23] V. Savchenko, C. Ferrigno, E. Kuulkers, A. Bazzano, E. Bozzo, B. Brandt, J. Chenevez, T. J. L. Courvoisier, R. Diehl, A. Domingo, L. Hanlon, E. Jourdain, A. von Kienlin, P. Laurent, F. Lebrun, A. Lutovinov, A. Martin-Carrillo, S. Mereghetti, L. Natalucci, J. Rodi, J. P. Roques, R. Sunyaev, and P. Ubertini, “INTEGRAL Detection of the First Prompt Gamma-Ray Signal Coincident with the Gravitational-wave Event GW170817,” *Astrophysical Journal Letters* **848**, L15 (2017), arXiv:1710.05449 [astro-ph.HE].
- [24] P. S. Cowperthwaite, E. Berger, V. A. Villar, B. D. Metzger, M. Nicholl, R. Chornock, P. K. Blanchard, W. Fong, R. Margutti, M. Soares-Santos, et al., “The Electromagnetic Counterpart of the Binary Neutron Star Merger LIGO/Virgo GW170817. II. UV, Optical, and Near-infrared Light Curves and Comparison to Kilonova Models,” *Astrophysical Journal Letters* **848**, L17 (2017).
- [25] E. Troja, L. Piro, H. van Eerten, R. T. Wollaeger, M. Im, O. D. Fox, N. R. Butler, S. B. Cenko, T. Sakamoto, C. L. Fryer, R. Ricci, A. Lien, R. E. Ryan, O. Korobkin, S. K. Lee, J. M. Burgess, W. H. Lee, A. M. Watson, C. Choi, S. Covino, P. D’Avanzo, C. J. Fontes, J. Becerra González, H. G. Khandrika, J. Kim, S. L. Kim, C. U. Lee, H. M. Lee, A. Kutyrev, G. Lim, R. Sánchez-Ramírez, S. Veilleux, M. H. Wieringa, and Y. Yoon, “The X-ray counterpart to the gravitational-wave event GW170817,” *Nature (London)* **551**, 71–74 (2017), arXiv:1710.05433 [astro-ph.HE].
- [26] V. A. Villar, J. Guillochon, E. Berger, B. D. Metzger, P. S. Cowperthwaite, M. Nicholl, K. D. Alexander, P. K. Blanchard, R. Chornock, T. Eftekhari, W. Fong, R. Margutti, and P. K. G. Williams, “The Combined Ultraviolet, Optical, and Near-infrared Light Curves of the Kilonova Associated with the Binary Neutron Star Merger GW170817: Unified Data Set, Analytic Models, and Physical Implications,” *Astrophysical Journal Letters* **851**, L21 (2017).
- [27] E. Pian, P. D’Avanzo, S. Benetti, M. Branchesi, E. Brocato, S. Campana, E. Cappellaro, S. Covino, V. D’Elia, J. P. U. Fynbo, et al., “Spectroscopic identification of r-process nucleosynthesis in a double neutron-star merger,” *Nature (London)* **551**, 67–70 (2017).
- [28] M. Nicholl, E. Berger, D. Kasen, B. D. Metzger, J. Elias, C. Briceño, K. D. Alexander, P. K. Blanchard, R. Chornock, P. S. Cowperthwaite, T. Eftekhari, W. Fong, R. Margutti, V. A. Villar, P. K. G. Williams, W. Brown, J. Annis, A. Bahramian, D. Brout, D. A. Brown, H.-Y. Chen, J. C. Clemens, E. Dennihy, B. Dunlap, D. E. Holz, E. Marchesini, F. Massaro, N. Moskowitz, I. Pelisoli, A. Rest, F. Ricci, M. Sako, M. Soares-Santos, and J. Strader, “The Electromagnetic Counterpart of the Binary Neutron Star Merger LIGO/Virgo GW170817. III. Optical and UV Spectra of a Blue Kilonova from Fast Polar Ejecta,” *Astrophysical Journal Letters* **848**, L18 (2017), arXiv:1710.05456 [astro-ph.HE].
- [29] Jonah M. Miller, Benjamin R. Ryan, Joshua C. Dolence, Adam Burrows, Christopher J. Fontes, Christopher L. Fryer, Oleg Korobkin, Jonas Lippuner, Matthew R. Mumpower, and Ryan T. Wollaeger, “Full transport model of GW170817-like disk produces a blue kilonova,” *Phys. Rev. D* **100**, 023008 (2019).
- [30] Masaomi Tanaka, Daiji Kato, Gediminas Gaigalas, and Kyohei Kawaguchi, “Systematic opacity calculations for kilonovae,” *Monthly Notices of the Royal Astronomical Society* **496**, 1369–1392 (2020), arXiv:1906.08914 [astro-ph.HE].
- [31] Jennifer Barnes, Y. L. Zhu, K. A. Lund, T. M. Sprouse, N. Vassh, G. C. McLaughlin, M. R. Mumpower, and R. Surman, “Kilonovae Across the Nuclear Physics Landscape: The Impact of Nuclear Physics Uncertainties on r-process-powered Emission,” *Astrophys. J.* **918**, 44 (2021), arXiv:2010.11182 [astro-ph.HE].
- [32] Y. L. Zhu, K. A. Lund, J. Barnes, T. M. Sprouse, N. Vassh, G. C. McLaughlin, M. R. Mumpower, and R. Surman, “Modeling Kilonova Light Curves: Dependence on Nuclear Inputs,” *Astrophys. J.* **906**, 94 (2021).
- [33] Oleg Korobkin, Ryan T. Wollaeger, Christopher L. Fryer, Aimee L. Hungerford, Stephan Rosswog, Christopher J. Fontes, Matthew R. Mumpower, Eve A. Chase, Wesley P. Even, Jonah Miller, G. Wendell Misch, and Jonas Lippuner, “Axisymmetric Radiative Transfer Models of Kilonovae,” *Astrophys. J.* **910**, 116 (2021).
- [34] A. Perego, S. Rosswog, R. M. Cabezón, O. Korobkin, R. Käppeli, A. Arcones, and M. Liebendörfer, “Neutrino-driven winds from neutron star merger remnants,” *Monthly Notices of the Royal Astronomical Society* **443**, 3134–3156 (2014), arXiv:1405.6730 [astro-ph.HE].
- [35] S. Rosswog, O. Korobkin, A. Arcones, F.-K. Thielemann, and T. Piran, “The long-term evolution of neutron star merger remnants - I. The impact of r-process nucleosynthesis,” *Monthly Notices of the Royal Astronomical Society* **439**, 744–756 (2014).
- [36] M. Ristic, E. Champion, R. O’Shaughnessy, R. Wollaeger, O. Korobkin, E. A. Chase, C. L. Fryer, A. L. Hungerford, and C. J. Fontes, “Interpolating detailed simulations of kilonovae: Adaptive learning and parameter inference applications,” *Physical Review Research* **4**, 013046 (2022), arXiv:2105.07013 [astro-ph.HE].
- [37] Ryan T. Wollaeger and Daniel R. van Rossum, “RADIATION TRANSPORT FOR EXPLOSIVE OUTFLOWS: OPACITY REGROUPING,” *The Astrophysical Journal Supplement Series* **214**, 28 (2014).
- [38] C. Winteler, R. Käppeli, A. Perego, A. Arcones, N. Vasset, N. Nishimura, M. Liebendörfer, and F. K. Thielemann, “Magnetorotationally Driven Supernovae as the Origin of Early Galaxy r-process Elements?” *Astrophysical Journal Letters* **750**, L22 (2012).
- [39] Jennifer Barnes, Daniel Kasen, Meng-Ru Wu, and Gabriel Martínez-Pinedo, “Radioactivity and Thermalization in the Ejecta of Compact Object Mergers and Their Impact on Kilonova Light Curves,” *The Astrophysical Journal* **829**, 110 (2016).

- [40] Ryan T Wollaeger, Oleg Korobkin, Christopher J Fontes, Stephan K Rosswog, Wesley P Even, Christopher L Fryer, Jesper Sollerman, Aimee L Hungerford, Daniel R van Rossum, and Allan B Wollaber, “Impact of ejecta morphology and composition on the electromagnetic signatures of neutron star mergers,” *Monthly Notices of the Royal Astronomical Society* **478**, 3298–3334 (2018), <https://academic.oup.com/mnras/article-pdf/478/3/3298/25067894/sty1018.pdf>.
- [41] C. J. Fontes, H. L. Zhang, J. Abdallah Jr., R. E. H. Clark, D. P. Kilcrease, J. Colgan, R. T. Cunningham, P. Hakel, N. H. Magee, and M. E. Sherrill, “The Los Alamos suite of relativistic atomic physics codes,” *Journal of Physics B Atomic Molecular Physics* **48**, 144014 (2015).
- [42] C. J. Fontes, C. L. Fryer, A. L. Hungerford, R. T. Wollaeger, and O. Korobkin, “A line-binned treatment of opacities for the spectra and light curves from neutron star mergers,” *Monthly Notices of the Royal Astronomical Society* **493**, 4143–4171 (2020).
- [43] J. Wofford, A. Yelikar, H. Gallagher, E. Champion, D. Wysocki, V. Delfavero, J. Lange, C. Rose, V. Valsan, S. Morisaki, J. Read, and R. O’Shaughnessy, “Expanding RIFT: Improving performance for GW parameter inference,” in prep..
- [44] A. G. W. Cameron, “Nuclear Reactions in Stars and Nucleogenesis,” *PASP* **69**, 201 (1957).
- [45] E. Margaret Burbidge, G. R. Burbidge, William A. Fowler, and F. Hoyle, “Synthesis of the elements in stars,” *Rev. Mod. Phys.* **29**, 547–650 (1957).
- [46] P. Möller, A. J. Sierk, T. Ichikawa, and H. Sagawa, “Nuclear ground-state masses and deformations: FRDM(2012),” *Atomic Data and Nuclear Data Tables* **109**, 1–204 (2016), [arXiv:1508.06294 \[nucl-th\]](https://arxiv.org/abs/1508.06294).
- [47] J. M. Pearson, N. Chamel, A. F. Fantina, and S. Goriely, “Symmetry energy: nuclear masses and neutron stars,” *European Physical Journal A* **50**, 43 (2014), [arXiv:1309.2783 \[nucl-th\]](https://arxiv.org/abs/1309.2783).
- [48] M. R. Mumpower, P. Jaffke, M. Verriere, and J. Randrup, “Primary fission fragment mass yields across the chart of nuclides,” *Phys. Rev. C* **101**, 054607 (2020), [arXiv:1911.06344 \[nucl-th\]](https://arxiv.org/abs/1911.06344).
- [49] I. V. Panov, I. Yu. Korneev, T. Rauscher, G. Martínez-Pinedo, A. Kelić-Heil, N. T. Zinner, and F. K. Thielemann, “Neutron-induced astrophysical reaction rates for translead nuclei,” *Astronomy and Astrophysics* **513**, A61 (2010), [arXiv:0911.2181 \[astro-ph.SR\]](https://arxiv.org/abs/0911.2181).
- [50] Trevor Sprouse, Matthew Mumpower, Rebecca Surman, and Ani Aprahamian, “A generalized framework for nucleosynthesis calculations,” in *APS Division of Nuclear Physics Meeting Abstracts*, APS Meeting Abstracts, Vol. 2015 (2015) p. EA.097.
- [51] S Rosswog, U Feindt, O Korobkin, M-R Wu, J Sollerman, A Goobar, and G Martinez-Pinedo, “Detectability of compact binary merger macronovae,” *Classical and Quantum Gravity* **34**, 104001 (2017).
- [52] David Radice, Albino Perego, Kenta Hotokezaka, Sebastiano Bernuzzi, Steven A. Fromm, and Luke F. Roberts, “Viscous-dynamical Ejecta from Binary Neutron Star Mergers,” *Astrophysical Journal Letters* **869**, L35 (2018), [arXiv:1809.11163 \[astro-ph.HE\]](https://arxiv.org/abs/1809.11163).
- [53] Rodrigo Fernández, Alexander Tchekhovskoy, Eliot Quataert, Francois Foucart, and Daniel Kasen, “Long-term GRMHD simulations of neutron star merger accretion discs: implications for electromagnetic counter-
- parts,” *Monthly Notices of the Royal Astronomical Society* **482**, 3373–3393 (2019), [arXiv:1808.00461 \[astro-ph.HE\]](https://arxiv.org/abs/1808.00461).
- [54] Vsevolod Nedora, Sebastiano Bernuzzi, David Radice, Boris Daszuta, Andrea Endrizzi, Albino Perego, Aviral Prakash, Mohammadtaher Safarzadeh, Federico Schianchi, and Domenico Logoteta, “Numerical Relativity Simulations of the Neutron Star Merger GW170817: Long-term Remnant Evolutions, Winds, Remnant Disks, and Nucleosynthesis,” *Astrophys. J.* **906**, 98 (2021), [arXiv:2008.04333 \[astro-ph.HE\]](https://arxiv.org/abs/2008.04333).
- [55] Claudio Arlandini, Franz Käppeler, Klaus Wisshak, Roberto Gallino, Maria Lugaro, Maurizio Busso, and Oscar Straniero, “Neutron Capture in Low-Mass Asymptotic Giant Branch Stars: Cross Sections and Abundance Signatures,” *Astrophys. J.* **525**, 886–900 (1999), [arXiv:astro-ph/9906266 \[astro-ph\]](https://arxiv.org/abs/astro-ph/9906266).
- [56] C. Sneden, J. J. Cowan, and R. Gallino, “Neutron-capture elements in the early galaxy,” *Annual Reviews of Astronomy and Astrophysics* **46**, 241–288 (2008).
- [57] Abdu Abohalima and Anna Frebel, “JINABase—A Database for Chemical Abundances of Metal-poor Stars,” *Astroph. J. S.* **238**, 36 (2018), [arXiv:1711.04410 \[astro-ph.SR\]](https://arxiv.org/abs/1711.04410).
- [58] Christopher Sneden, John J. Cowan, James E. Lawler, Inese I. Ivans, Scott Burles, Timothy C. Beers, Francesca Primas, Vanessa Hill, James W. Truran, George M. Fuller, Bernd Pfeiffer, and Karl-Ludwig Kratz, “The Extremely Metal-poor, Neutron Capture-rich Star CS 22892-052: A Comprehensive Abundance Analysis,” *Astrophys. J.* **591**, 936–953 (2003), [arXiv:astro-ph/0303542 \[astro-ph\]](https://arxiv.org/abs/astro-ph/0303542).
- [59] W. Hayek, U. Wiesendahl, N. Christlieb, K. Eriksson, A. J. Korn, P. S. Barklem, V. Hill, T. C. Beers, K. Farouqi, B. Pfeiffer, and K.-L. Kratz, “The Hamburg/ESO R-process enhanced star survey (HERES). IV. Detailed abundance analysis and age dating of the strongly r-process enhanced stars CS 29491-069 and HE 1219-0312,” *Astronomy and Astrophysics* **504**, 511–524 (2009), [arXiv:0910.0707 \[astro-ph.SR\]](https://arxiv.org/abs/0910.0707).
- [60] V. Hill, B. Plez, R. Cayrel, T. C. Beers, B. Nordström, J. Andersen, M. Spite, F. Spite, B. Barbuy, P. Bonifacio, E. Depagne, P. François, and F. Primas, “First stars. I. The extreme r-element rich, iron-poor halo giant CS 31082-001. Implications for the r-process site(s) and radioactive cosmochronology,” *Astronomy and Astrophysics* **387**, 560–579 (2002), [astro-ph/0203462](https://arxiv.org/abs/astro-ph/0203462).
- [61] J. Westin, C. Sneden, B. Gustafsson, and J. J. Cowan, “The r-Process-enriched Low-Metallicity Giant HD 115444,” *Astrophys. J.* **530**, 783–799 (2000), [astro-ph/9910376](https://arxiv.org/abs/astro-ph/9910376).
- [62] I. I. Ivans, J. Simmerer, C. Sneden, J. E. Lawler, J. J. Cowan, R. Gallino, and S. Bisterzo, “Near-Ultraviolet Observations of HD 221170: New Insights into the Nature of r-Process-rich Stars,” *Astrophys. J.* **645**, 613–633 (2006), [astro-ph/0604180](https://arxiv.org/abs/astro-ph/0604180).
- [63] J. J. Cowan, C. Sneden, S. Burles, I. I. Ivans, T. C. Beers, J. W. Truran, J. E. Lawler, F. Primas, G. M. Fuller, B. Pfeiffer, and K.-L. Kratz, “The Chemical Composition and Age of the Metal-poor Halo Star BD +17deg3248,” *Astrophys. J.* **572**, 861–879 (2002), [astro-ph/0202429](https://arxiv.org/abs/astro-ph/0202429).
- [64] J Heinzl, M W Coughlin, T Dietrich, M Bulla, S Antier, N Christensen, D A Coulter, R J Foley, L Issa, and

- N Khetan, “Comparing inclination-dependent analyses of kilonova transients,” *Monthly Notices of the Royal Astronomical Society* **502**, 3057–3065 (2021).
- [65] Michael W. Coughlin, Tim Dietrich, Zoheyr Doctor, Daniel Kasen, Scott Coughlin, Anders Jerkstrand, Giorgos Leloudas, Owen McBrien, Brian D. Metzger, Richard O’Shaughnessy, and Stephen J. Smartt, “Constraints on the neutron star equation of state from AT2017gfo using radiative transfer simulations,” *Monthly Notices of the Royal Astronomical Society* **480**, 3871–3878 (2018).
- [66] Michael W. Coughlin, Tim Dietrich, Ben Margalit, and Brian D. Metzger, “Multimessenger Bayesian parameter inference of a binary neutron star merger,” *Monthly Notices of the Royal Astronomical Society* **489**, L91–L96 (2019).
- [67] S. J. Smartt, T. W. Chen, A. Jerkstrand, M. Coughlin, E. Kankare, S. A. Sim, M. Fraser, C. Inerra, K. Maguire, K. C. Chambers, *et al.*, “A kilonova as the electromagnetic counterpart to a gravitational-wave source,” *Nature (London)* **551**, 75–79 (2017).
- [68] Matteo Breschi, Albino Perego, Sebastiano Bernuzzi, Walter Del Pozzo, Vsevolod Nedora, David Radice, and Diego Vescovi, “At2017gfo: Bayesian inference and model selection of multicomponent kilonovae and constraints on the neutron star equation of state,” *Monthly Notices of the Royal Astronomical Society* **505**, 1661–1677 (2021).
- [69] Matt Nicholl, Ben Margalit, Patricia Schmidt, Graham P Smith, Evan J Ridley, and James Nuttall, “Tight multimessenger constraints on the neutron star equation of state from gw170817 and a forward model for kilonova light-curve synthesis,” *Monthly Notices of the Royal Astronomical Society* **505**, 3016–3032 (2021).
- [70] K. Lukošiuėte, G. Raaijmakers, Z. Doctor, M. Soares-Santos, and B. Nord, “KilonovaNet: Surrogate models of kilonova spectra with conditional variational autoencoders,” *Monthly Notices of the Royal Astronomical Society* **516**, 1137–1148 (2022), arXiv:2204.00285 [astro-ph.IM].
- [71] Mouza Almualla, Yuhong Ning, Mattia Bulla, Tim Dietrich, Michael W. Coughlin, and Nidhal Gues-soum, “Using Neural Networks to Perform Rapid High-Dimensional Kilonova Parameter Inference,” arXiv e-prints, arXiv:2112.15470 (2021), arXiv:2112.15470 [astro-ph.HE].
- [72] Kyohei Kawaguchi, Masaru Shibata, and Masaomi Tanaka, “Diversity of Kilonova Light Curves,” *Astrophys. J.* **889**, 171 (2020).
- [73] David Radice, Filippo Galeazzi, Jonas Lippuner, Luke F. Roberts, Christian D. Ott, and Luciano Rezzolla, “Dynamical mass ejection from binary neutron star mergers,” *Monthly Notices of the Royal Astronomical Society* **460**, 3255–3271 (2016), arXiv:1601.02426 [astro-ph.HE].
- [74] Tim Dietrich, Sebastiano Bernuzzi, Maximiliano Ujevic, and Wolfgang Tichy, “Gravitational waves and mass ejecta from binary neutron star mergers: Effect of the stars’ rotation,” *Phys. Rev. D* **95**, 044045 (2017).
- [75] Masaru Shibata and Kenta Hotokezaka, “Merger and Mass Ejection of Neutron Star Binaries,” *Annual Review of Nuclear and Particle Science* **69**, 41–64 (2019), arXiv:1908.02350 [astro-ph.HE].
- [76] E Troja, H van Eerten, B Zhang, G Ryan, L Piro, R Ricci, B O’Connor, M H Wieringa, S B Cenko, and T Sakamoto, “A thousand days after the merger: Continued X-ray emission from GW170817,” *Monthly Notices of the Royal Astronomical Society* **498**, 5643–5651 (2020).
- [77] P. A. Evans, S. B. Cenko, J. A. Kennea, S. W. K. Emery, N. P. M. Kuin, O. Korobkin, R. T. Wollaeger, C. L. Fryer, K. K. Madsen, F. A. Harrison, *et al.*, “ $\text{ij}_{\text{swift}}$ / $\text{ij}$  and  $\text{ij}_{\text{nustar}}$ / $\text{ij}$  observations of gw170817: Detection of a blue kilonova,” *Science* **358**, 1565–1570 (2017), <https://www.science.org/doi/pdf/10.1126/science.aap9580>.
- [78] Elias R. Most, L. Jens Papenfort, Samuel D. Toote, and Luciano Rezzolla, “On accretion discs formed in MHD simulations of black hole-neutron star mergers with accurate microphysics,” *Monthly Notices of the Royal Astronomical Society* **506**, 3511–3526 (2021), arXiv:2106.06391 [astro-ph.HE].
- [79] Vsevolod Nedora, Federico Schianchi, Sebastiano Bernuzzi, David Radice, Boris Daszuta, Andrea Endrizzi, Albino Perego, Aviral Prakash, and Francesco Zappa, “Mapping dynamical ejecta and disk masses from numerical relativity simulations of neutron star mergers,” *Classical and Quantum Gravity* **39**, 015008 (2022).
- [80] Alexander P. Ji, Maria R. Drout, and Terese T. Hansen, “The Lanthanide Fraction Distribution in Metal-poor Stars: A Test of Neutron Star Mergers as the Dominant r-process Site,” *Astrophys. J.* **882**, 40 (2019), arXiv:1905.01814 [astro-ph.HE].
- [81] K. Farouqi, F. K. Thielemann, S. Rosswog, and K. L. Kratz, “Correlations of r-process elements in very metal-poor stars as clues to their nucleosynthesis sites,” *Astronomy and Astrophysics* **663**, A70 (2022), arXiv:2107.03486 [astro-ph.SR].
- [82] Sho Fujibayashi, Kenta Kiuchi, Shinya Wanajo, Koutarou Kyutoku, Yuichiro Sekiguchi, and Masaru Shibata, “Comprehensive study on the mass ejection and nucleosynthesis in the binary neutron star mergers leaving short-lived massive neutron stars,” arXiv e-prints, arXiv:2205.05557 (2022), arXiv:2205.05557 [astro-ph.HE].
- [83] Nicole Vassh, Gail C. McLaughlin, Matthew R. Mumpower, and Rebecca Surman, “The need for a local nuclear physics feature in the neutron-rich rare-earths to explain solar r-process abundances,” arXiv e-prints, arXiv:2202.09437 (2022), arXiv:2202.09437 [nucl-th].
- [84] I. Kullmann, S. Goriely, O. Just, R. Ardevol-Pulpillo, A. Bauswein, and H. T. Janka, “Dynamical ejecta of neutron star mergers with nucleonic weak processes I: nucleosynthesis,” *Monthly Notices of the Royal Astronomical Society* **510**, 2804–2819 (2022), arXiv:2109.02509 [astro-ph.HE].